MATHEMATICAL MODELING AND COMPUTING, Vol. 10, No. 4, pp. 1250–1259 (2023)

Heat transfer analysis on magneto–ternary nanofluid flow in a porous medium over a moving surface

Anuar N. S.[1], Hussain B. N.[1], Asuki N. A. M.[1], Bachok N.[2,3]

[1] *School of Mathematical Sciences, College of Computing, Informatics and Mathematics, University Technology MARA, 40450 Shah Alam, Selangor, Malaysia*
[2] *Institute for Mathematical Research, University Putra Malaysia, 43400 Serdang, Selangor, Malaysia*
[3] *Department of Mathematics and Statistics, Faculty of Science, University Putra Malaysia, 43400 Serdang, Selangor, Malaysia*

(Received 26 September 2023; Revised 18 November 2023; Accepted 19 November 2023)

Researchers have become attracted with ternary hybrid nanoparticles because of its effectiveness in enhancing heat transfer and have gone on to further analyze the working fluid. This study is focusing on magneto-ternary nanofluid flow in a porous medium over a moving plate with Joule heating. The combination of TiO_2, SiO_2, and Al_2O_3 with water, H_2O, as the based fluid is used for the analysis. Using similarity transformation, the complexity of partial differential equations (PDEs) is reduced into ordinary differential equation (ODE) systems, which are then numerically solved in MATLAB using the bvp4c function for various values of the governing parameters. The impacts of different dimensionless physical parameters on velocity, temperature as well as skin friction coefficient and local Nusselt number are reported in the form of graphs. Two solutions are achieved when the plate and free-stream are moving along mutually opposite directions. Further, local Nusselt number increases with permeability parameter and suction parameter. Also, increments in permeability parameter and the suction parameter lead to the delay in the boundary layer separation. Furthermore, by combining TiO_2 with a volume percentage of SiO_2-Al_2O_3/H_2O, the heat transfer is enhanced. With an increase in nanoparticle volume fraction, the similarity solutions to exist decrease.

Keywords: *ternary nanofluid; boundary layer flow; heat transfer; porous medium; moving plate.*

2010 MSC: 76D05, 76D10, 76W05 **DOI:** 10.23939/mmc2023.04.1250

1. Introduction

In the past few years, the use of nanofluids as a conventional fluid that can enhance heat transfer has attracted considerable attention among engineers around the world. 'Nanofluid' term was first proposed by Choi [1] that includes an explanation of how the dispersion of nanoparticles in based fluids like water, ethylene glycol, and propylene glycol happens. Subsequently, Suresh et al. [2] conducted experimental work on improving the thermal conductivity of a based fluid by mixing two different types of nanofluids into the based fluid. They discussed the advantages of using the hybrid nanofluid and led Devi and Devi [3] to analyze the boundary layer flow problem in hybrid nanofluid. Huminic and Huminic [4] demonstrated through both experimental and numerical investigations that the utilization of hybrid nanofluids leads to an increase in thermal conductivity. Their findings suggest that this enhancement in heat transfer performance could have practical applications in improving the efficiency of heat exchangers.

However, in recent years, researchers have been focusing on a newly categorized class of functional fluids known as ternary nanofluids. These fluids consist of a conventional fluid infused with three

This work was supported by MyRA Research Grant (600-RMC 5/3/GPM (035/2022)) and School of Mathematical Sciences, College of Computing, Informatics and Mathematics, University Technology MARA.

distinct solid nanoparticles. These nanoparticles can encompass a variety of materials, ranging from metals, non-metals, metal oxides, carbon nanotubes, to various combinations thereof. Due to the fact that the trihybrid nanofluid combines various chemical bonds to enhance heat transfer and since each nanoparticle has a chemical bond with its own unique features, it has greater heat transfer capabilities than the other. Manjunatha et al. [5] then discovered a ternary nanofluid in order to improve thermal conductivity by adding another nanoparticle into a hybrid nanofluid. They analyzed the heat transfer characteristics and flow behavior of the combination of titanium dioxide TiO_2, silicon dioxide SiO_2, and aluminum oxide Al_2O_3 as the nanoparticles and water H_2O. It was proven that it has better heat transfer properties than base fluid, nanofluid, and hybrid nanofluid. Using the Laplace transform technique, Shah et al. [6] examined the flow behavior of the second-grade fluid containing a ternary nanoparticle suspension in a vertical plate. Because of its significant features, ternary nanofluid is well-known and valuable among researchers [7, 8] and [9].

Boundary layer flow across porous media is harnessed for a diverse range of purposes in chemical, civil, and mechanical engineering. Characterized by properties such as porosity and permeability, a porous medium is a material containing fluid-filled pores. Porosity quantifies the material's fluid retention capacity, and these applications encompass tasks like controlling the temperature of electronic devices through heating and cooling, generating renewable energy, providing insulation for buildings against external elements, and studying geological systems. Kameswaran et al. [10] and Eid and Mahny [11] elucidated that an increase in the permeability parameter of the porous material, in which the flow over an expanding surface occurs, leads to a reduction in momentum thickness while causing the thermal boundary layer to expand. Kausar et al. [12] numerically investigated the laminar two-dimensional heat transfer flow of micropolar nanofluid through a porous medium with viscous dissipation and thermal radiation that contains copper over a stretching sheet. The study proved that using nanofluid through a porous medium grew the width of the thermal boundary layer. Zeeshan et al. [13] investigated the electro-magnetized suspensions in engine-oil and water-based Newtonian liquids flowing through the porous space.

Since the ground-breaking Blasius research, numerous studies were published on the boundary layer problem. The Blasius flow was then explored by Abu-Sitta [14], who discovered the existence of a solution. Later on, the method of Adomian decomposition was applied by Wang [15] to the classical Blasius equation, followed by Cortell [16], who looked numerically at the Blasius equation. Unlike Blasius, Sakiadis considered boundary layer flow towards a moving flat surface, claiming that there were similar ordinary differential equations (ODEs) to Blasius, with different boundary conditions. Since then, several studies (including Idris et al. [17], Samat et al. [18] and Aminuddin et al. [19]) scrutinized the fluid flowing on a moving plate and stated that duality existed when the plate and free stream traveled oppositely.

In all the studies cited above, it is discovered that the behavior of boundary layer flow of a ternary nanofluid past a moving surface in a porous medium has yet to be investigated. Thus, a numerical study inspired by Khashi'ie et al. [20] is presented by broadening their knowledge by including new control parameter such as porous medium in ternary nanofluid. The boundary layer partial differential equations are converted into a system of ordinary differential equations using the proper similarity transformation. MATLAB is utilized to create numerical outcomes, which are then depicted using a variety of charts and diagrams. The key findings are visually presented and organized in tables before undergoing thorough analysis. The outcomes of the current study on the flow behavior of ternary nanofluid in moving surfaces are anticipated to provide valuable insights for academics, engineers, and researchers. This knowledge will enable them to better understand the characteristics of this fluid and make predictions about its properties, thereby exploring potential applications in diverse industrial and engineering processes.

2. Mathematical formulation

Consider the boundary layer flow of an incompressible ternary TiO_2-SiO_2-Al_2O_3/H_2O nanofluid past a permeable flat plate as shown in Figure 1. The Cartesian coordinates are labeled as x and y, where the x-axis measured along the plate and $y-$axis is normal to it and the flow is being in the region $y \geqslant 0$. The ternary nanofluid's free stream has a constant velocity U. An uniform magnetic field of strength $\beta = \beta_0 x^{1/2}$ is imposed normal to a moving plate embedded in a porous medium where β is the magnetic field. The plate is moving with the velocity $U\lambda$, where λ indicates the moving parameters, which $\lambda > 0$ means that the same path between the moving plate and free stream and $\lambda < 0$ indicates different orientation, respectively. The moving plate temperature is T_w, while the temperature of the far field is T_∞.

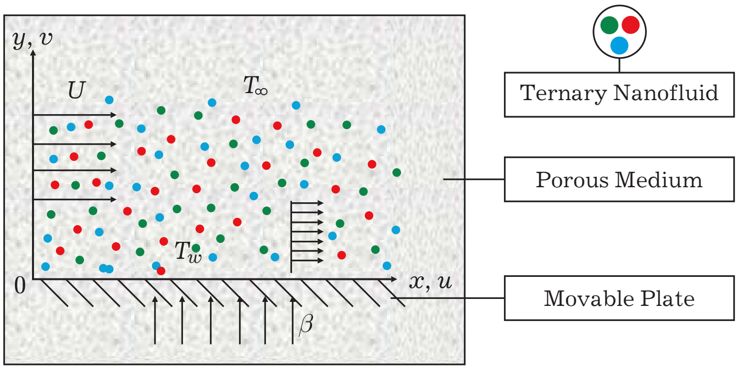

Fig. 1. Physical illustrations with coordinates system.

Under these assumptions, the governing boundary layer equations consist of continuity, momentum, and energy ternary nanofluids can be written as (see [3, 20, 21]):

$$\frac{\partial u}{\partial x} + \frac{\partial u}{\partial y} = 0, \tag{1}$$

$$u\frac{\partial u}{\partial x} + v\frac{\partial u}{\partial y} = \frac{\mu_{thnf}}{\rho_{thnf}}\frac{\partial^2 u}{\partial y^2} - \frac{\sigma_{thnf}}{\rho_{thnf}}\beta^2 (u - U) - \frac{\mu_{thnf}}{K\rho_{thnf}}(u - U), \tag{2}$$

$$u\frac{\partial T}{\partial x} + v\frac{\partial T}{\partial y} = \frac{k_{thnf}}{(\rho C_p)_{thnf}}\frac{\partial^2 T}{\partial y^2} + \frac{\sigma_{thnf}}{(\rho C_p)_{thnf}}\beta^2 (u - U)^2. \tag{3}$$

The associate boundary conditions are:

$$\begin{gathered} u = \lambda U, \quad v = v_w, \quad T = T_w \quad \text{at} \quad y = 0, \\ u \to U, \quad T \to T_\infty \quad \text{as} \quad y \to \infty. \end{gathered} \tag{4}$$

Here, u and v are the velocity components along the x and y axes, respectively. The subscript $thnf$ is ternary hybrid nanofluid. σ is electrical conductivity of the fluid, T is the temperature, C_p is the specific heat at constant pressure, ρ is the density, μ is the dynamic viscosity, $K = K_0 x$ is the permeability of porous medium and k is the thermal conductivity. The mass fluid velocity is assumed to be $v_w = -\sqrt{\frac{U\nu_f}{2x}}S$, where S is the initial strength of suction, $v_w < 0$ for suction and $v_w > 0$ for injection, respectively.

This study considers the laminar flow of an incompressible ternary nanofluid created by suspending TiO_2, Al_2O_3, and SiO_2 in water. The reaction between alumina and sulphuric acid results in acid sites that are weaker in strength. The nanoparticle composition will become stable and chemically inert due to these newly created acid sites. The goal of this research is to create a coolant that uses TiO_2 to cool the device. To improve the rate of heat transmission, additional experimental research on ternary nanofluid needs to be carried out. In this present work, the combination of TiO_2, Al_2O_3, and SiO_2 with water-based forms of ternary nanofluid. Here, ϕ_1 indicates TiO_2 nanoparticle, ϕ_2 and ϕ_3 denote SiO_2 and Al_2O_3 nanoparticles, respectively. The range value for ϕ_1, ϕ_2 and ϕ_3 were set up between 0 and 0.01, in which $\phi_1 = \phi_2 = \phi_3 = 0$ implies regular base fluid (H_2O), $\phi_3 = 0.01$ and $\phi_2 = \phi_3 = 0.01$ implies nanofluid and hybrid nanofluid, whereas $\phi_1 = \phi_2 = \phi_3 = 0.01$ signifies ternary nanofluid. The thermophysical properties of TiO_2-SiO_2-Al_2O_3/H_2O ternary nanofluid (see [5]) are given in Table 1. The thermophysical constants of the nanoparticles and base fluid (see [5, 20, 22]) are given in Table 2.

Table 1. Correlation on thermophysical properties of ternary nanofluid.

Properties	Ternary nanofluid
Density	$\rho_{thnf} = (1-\phi_1)\{(1-\phi_2)[(1-\phi_3)\rho_f + \phi_3\rho_3] + \phi_2\rho_2\} + \phi_1\rho_1$
Heat capacity	$(\rho C_p)_{thnf} = (1-\phi_1)\left\{(1-\phi_2)\left[(1-\phi_3)(\rho C_p)_f + \phi_3(\rho C_p)_3\right] + \phi_2(\rho C_p)_2\right\} + \phi_1(\rho C_p)_1$
Viscosity	$\mu_{thnf} = \dfrac{\mu_f}{(1-\phi_1)^{2.5}(1-\phi_2)^{2.5}(1-\phi_3)^{2.5}}$
Thermal conductivity	$\dfrac{k_{thnf}}{k_{hnf}} = \dfrac{k_1 + 2k_{hnf} - 2\phi_1(k_{hnf} - k_1)}{k_1 + 2k_{hnf} + \phi_1(k_{hnf} - k_1)}$, where $\dfrac{k_{hnf}}{k_{nf}} = \dfrac{k_2 + 2k_{nf} - 2\phi_2(k_{nf} - k_2)}{k_2 + 2k_{nf} + \phi_2(k_{nf} - k_2)}$ and $\dfrac{k_{nf}}{k_f} = \dfrac{k_3 + 2k_f - 2\phi_3(k_f - k_3)}{k_3 + 2k_f + \phi_3(k_f - k_3)}$
Electrical conductivity	$\dfrac{\sigma_{thnf}}{\sigma_{hnf}} = \dfrac{(1+2\phi_1)\sigma_1 + (1-2\phi_1)\sigma_{hnf}}{(1-\phi_1)\sigma_1 + (1+\phi_1)\sigma_{hnf}}$, where $\dfrac{\sigma_{hnf}}{\sigma_{nf}} = \dfrac{(1+2\phi_2)\sigma_2 + (1-2\phi_2)\sigma_{nf}}{(1-\phi_2)\sigma_2 + (1+\phi_2)\sigma_{nf}}$ and $\dfrac{\sigma_{nf}}{\sigma_f} = \dfrac{(1+2\phi_3)\sigma_3 + (1-2\phi_3)\sigma_f}{(1-\phi_3)\sigma_3 + (1+\phi_3)\sigma_f}$

Table 2. Thermophysical properties of the nanoparticles and the base fluid.

	$\rho[\mathrm{kg\,m^{-3}}]$	$C_p[\mathrm{J(kg\,K)^{-1}}]$	$\sigma[\mathrm{S\,m^{-1}}]$	$k[\mathrm{W(mK)^{-1}}]$
H_2O	997.1	4179	0.05	0.613
TiO_2	4250	686.2	2.4×10^6	8.9538
SiO_2	2270	730	3.5×10^6	1.4013
Al_2O_3	3970	765	1×10^{-10}	40
Cu	8933	385	5.96×10^7	401

The following similarity transformation is introduced as below [20]:

$$\eta = y\sqrt{\frac{U}{2x\nu_f}}, \quad \psi = \sqrt{2\nu_f x U}\, f(\eta), \quad \theta(\eta) = \frac{T - T_\infty}{T_w - T_\infty}, \tag{5}$$

where η is the independent similarity variable, ψ is the stream function, f and θ are the dimensionless velocity and temperature, respectively. Using the Equation (5), Equations (1)–(3) together with the boundary conditions (4) are transformed as below:

$$\left(\frac{\mu_{thnf}/\mu_f}{\rho_{thnf}/\rho_f}\right) f''' + f''f - \left(\frac{\sigma_{thnf}/\sigma_f}{\rho_{thnf}/\rho_f}\right) M(f'-1) - \left(\frac{\mu_{thnf}/\mu_f}{\rho_{thnf}/\rho_f}\right)\kappa(f'-1) = 0, \tag{6}$$

$$\left(\frac{k_{thnf}/k_f}{(\rho C_p)_{thnf}/(\rho C_p)_f}\right)\frac{1}{\mathrm{Pr}}\theta'' + f\theta' + \mathrm{Ec}\, M\left(\frac{\sigma_{thnf}/\sigma_f}{(\rho C_p)_{thnf}/(\rho C_p)_f}\right)(f'-1)^2 = 0 \tag{7}$$

along with the boundary conditions:

$$\begin{gathered} f(0) = S, \quad f'(0) = \lambda, \quad \theta(0) = 1, \\ f'(\eta) \to 1, \quad \theta(\eta) \to 0 \quad \text{as} \quad \eta \to \infty. \end{gathered} \tag{8}$$

Here, M denoted as magnetic field, κ is permeability and Ec is Eckert number given as

$$M = \frac{2\beta_0^2\sigma_f}{U\rho_f}, \quad \kappa = \frac{2\mu_f}{UK_0\rho_f}, \quad \mathrm{Ec} = \frac{U^2}{(C_p)_f(T_w - T_\infty)}. \tag{9}$$

The attentiveness study for this problem is skin friction Cf_x and Nusselt number Nu_x. Both can be represented as

$$\mathrm{Cf}_x = \frac{\mu_{thnf}}{\rho_f U^2}\left[\frac{\partial u}{\partial y}\right]_{y=0}, \quad \mathrm{Nu}_x = -x\frac{k_{thnf}}{k_f(T_w - T_\infty)}\left[\frac{\partial T}{\partial y}\right]_{y=0}. \tag{10}$$

By using Equation (5), Equation (10) are transformed into

$$\sqrt{2}\,\mathrm{Re}_x^{\frac{1}{2}}\,\mathrm{Cf}_x = \frac{\mu_{thnf}}{\mu_f}f''(0), \quad \sqrt{2}\,\mathrm{Re}_x^{-\frac{1}{2}}\,\mathrm{Nu}_x = -\frac{k_{thnf}}{k_f}\theta'(0), \tag{11}$$

where $\mathrm{Re}_x = \frac{Ux}{\nu_f}$ is the local Reynold number.

3. Validation test

Table 3. Comparison values of $f''(0)$ and $-\theta'(0)$ for $\phi = 0$ (pure fluid) with various values of λ and $\mathrm{Pr} = 6.2$.

λ	Present Result		Rohni et al. [23]	
	$f''(0)$	$-\theta'(0)$	$f''(0)$	$-\theta'(0)$
-0.10	0.461049	0.701102	0.4611	0.7012
	[0.001924]	[0.000000]	[0.0019]	[0.0000]
-0.15	0.449074	0.602170	0.4491	0.6023
	[0.008657]	[0.000000]	[0.0087]	[0.0000]
-0.20	0.430151	0.493436	0.4302	0.4935
	[0.022185]	[0.000000]	[0.0222]	[0.0000]
-0.25	0.401524	0.372005	0.4015	0.3721
	[0.045390]	[0.000004]	[0.0454]	[0.0000]
-0.30	0.356638	0.233101	0.3567	0.2332
	[0.084871]	[0.000170]	[0.0849]	[0.0002]
-0.35	0.257581	0.058647	0.2578	0.0588
	[0.178558]	[0.009877]	[0.1785]	[0.0099]
'[ ]' Second solution				

Before generating the solutions, a few validation tests were needed and conducted with previous similar studies from Khashi'ie et al. [20] and Rohni et al. [23] to verify the accuracy of the present results as shown in Tables 3 and 4, respectively. Using bvp4c solver built-in MATLAB, Equations (6)–(8) are computed. Table 3 shows the comparison values of $f''(0)$ and $-\theta'(0)$ for various values of λ when $\phi_1 = \phi_2 = \phi_3 = 0$, while Table 4 shows the values of $f''(0)$ when $\mathrm{Cu} = 0.1$ and $M = S = 0$. The validation test was perfect since the present results compared are all within the acceptable range. Hence, it is satisfactory to assume that the results are reliable.

Table 4. Comparison values of $f''(0)$ when $\mathrm{Cu} = 0.1$ and $M = S = 0$ with various values of λ.

λ	Present Result	Khashi'ie et al. [20]	Rohni et al. [23]
-0.10	0.541615	0.541615	0.5416
	[0.002274]	[0.002274]	[0.0023]
-0.15	0.527547	0.527547	0.5276
	[0.010169]	[0.010169]	[0.0102]
-0.20	0.505318	0.505318	0.5053
	[0.026061]	[0.026061]	[0.0261]
-0.25	0.471688	0.471688	0.4717
	[0.053322]	[0.053322]	[0.0533]
-0.30	0.418959	0.418959	0.4190
	[0.099702]	[0.099702]	[0.0997]
-0.35	0.302592	0.302592	0.3028
	[0.209761]	[0.209761]	[0.2098]
-0.3541	0.257961	0.257961	0.2623
	[0.253877]	[0.253877]	[-]
'[ ]' Second solution			

4. Analysis of result

The discussion on the results of physical interest towards the governing parameters examined for this study is elaborated in this section. The sequel to the graphical results is obtained by computing Equations (6)–(8) into the bvp4c, MATLAB. Figures 2 and 3 highlight the distribution of skin friction coefficient $\sqrt{2}\,\mathrm{Re}_x^{1/2}C_f$ and local Nusselt number $\sqrt{2}\,\mathrm{Re}_x^{-1/2}\mathrm{Nu}_x$ towards a moving parameter λ for various values of S when $\phi_1 = \phi_2 = \phi_3 = 0.01$. For $S = 0$, 0.2, 0.4, the range wherein the various arrangements exists (or possible) is specified by $\lambda_c = -0.38674 \leqslant \lambda \leqslant 1.5$, $\lambda_c = -0.51759 \leqslant \lambda \leqslant 1.5$ and $\lambda_c = -0.66759 \leqslant \lambda \leqslant 1.5$, i.e., these multiple solutions illustrate an expanding conduct with inspiring the estimations of S. Here, λ_c denotes the critical value for λ where there is no solutions for $\lambda < \lambda_c$. The solid lines exhibit upper branch (first) solution, whereas dotted lines demonstrate lower branch (second) solution. The connection between the dual-type solutions is established through the critical value λ_c, which becomes the point of separation of the solutions as well as the boundary layer. It is found that by the increment value of S, the range of solutions widens. The first solution exhibits a significant variation, whereas the second one shows a minimal difference. At $\lambda = 1$, the skin friction is not produced because both the plate and the free stream of the ternary nanofluid move at an equal velocity. The skin friction coefficient values demonstrate an increase for $\lambda < 1$ up to a certain value and then begin to decrease after this value. Suction removes fluid near the surface, creating a region of lower pressure. This pressure gradient can accelerate the main flow towards the surface, which, in turn, can increase the momentum of the fluid particles in the boundary layer, leading to higher skin friction. The effect of suction S increases fluid velocity near the surface. This enhanced fluid motion results in a higher rate of heat exchange between the surface and the fluid as portrayed in Figure 3. As fluid particles move more vigorously, they carry away heat from the surface more effectively.

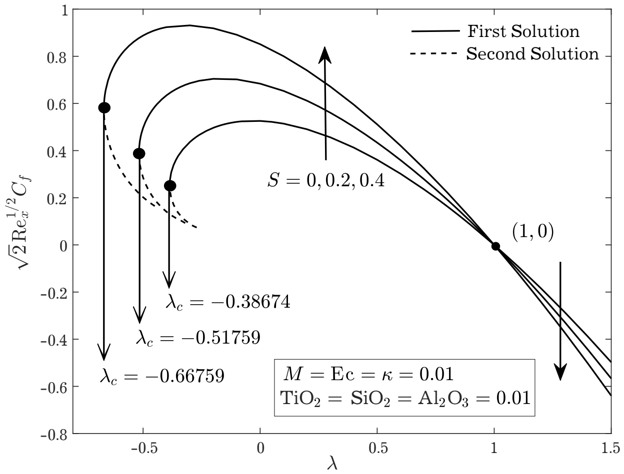

Fig. 2. Skin friction coefficient with various S.

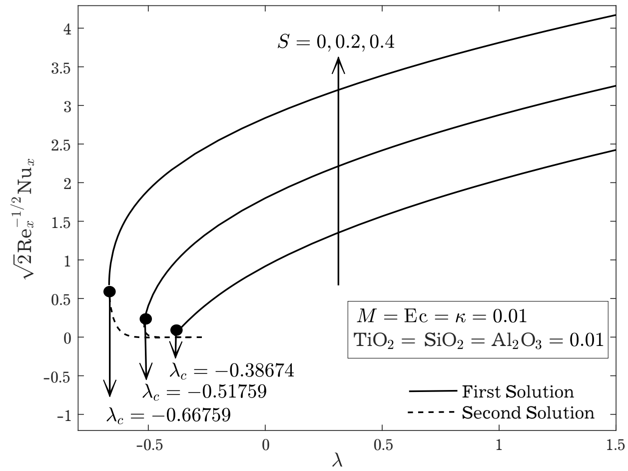

Fig. 3. Local Nusselt number with various S.

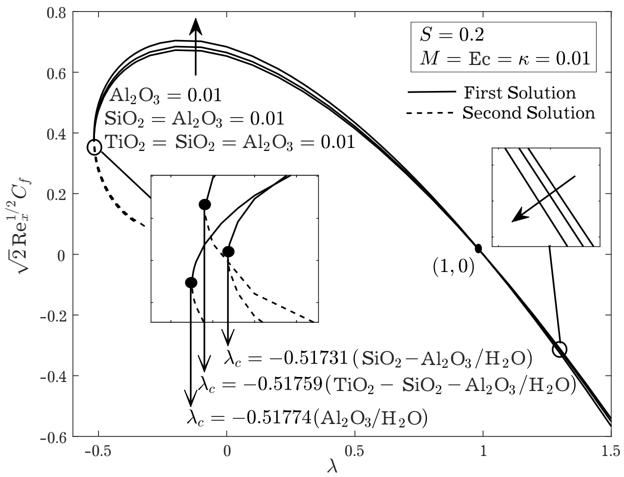

Fig. 4. Skin friction coefficient with various ϕ.

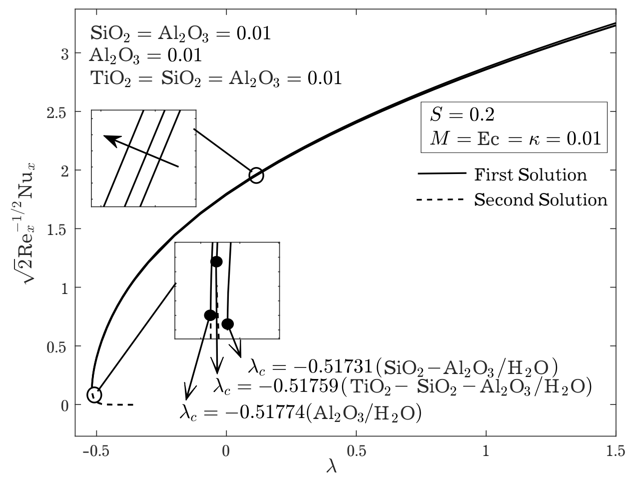

Fig. 5. Local Nusselt number with various ϕ.

Figures 4 and 5 show the variations of skin friction coefficient $\sqrt{2}\,\mathrm{Re}_x^{1/2}C_f$ and local Nusselt number $\sqrt{2}\,\mathrm{Re}_x^{-\frac{1}{2}}\mathrm{Nu}_x$ with different types of nanofluids, i.e., $\phi_3 = 0.01$ ($\mathrm{Al_2O_3/H_2O}$), $\phi_2 = \phi_3 = 0.01$ ($\mathrm{SiO_2}$-$\mathrm{Al_2O_3/H_2O}$) and $\phi_1 = \phi_2 = \phi_3 = 0.01$ ($\mathrm{TiO_2}$-$\mathrm{SiO_2}$-$\mathrm{Al_2O_3/H_2O}$). According to these figures, the upper branch of the results increases as nanoparticle volume fraction ϕ increases. These graphs demonstrated the existence of dual solutions for $\lambda_c < \lambda < 0$, such that the corresponding critical points of $\phi_3 = 0.01$, $\phi_2 = \phi_3 = 0.01$ and $\phi_1 = \phi_2 = \phi_3 = 0.01$ are $\lambda_c = -0.51774$, $\lambda_c = -0.51731$ and $\lambda_c = -0.51759$. These graphical results describe that boosting the nanoparticle volume fraction parameter fastens the separation of the boundary layer. Moreover, it is found that with an increment in the nanoparticle volume fraction, skin friction enhances when $\lambda < 1$ for the upper branch. Physically, the elevated viscosity due to more nanoparticles leads to increased skin friction by creating higher shear stress and drag. Figures 5 displayed that ternary nanofluid has a better heat transfer rate compared to the hybrid nanofluid and mono nanofluid due to a higher value in $\sqrt{2}\,\mathrm{Re}_x^{-1/2}\mathrm{Nu}_x$. This indicates ternary nanofluid has a thinner thermal boundary layer thickness, which may produce a larger heat flux and enhance the heat transfer rate. The enhanced convective heat transfer resulting from improved effective thermal conductivity and heat capacity leads to higher heat transfer coefficients and local Nusselt numbers.

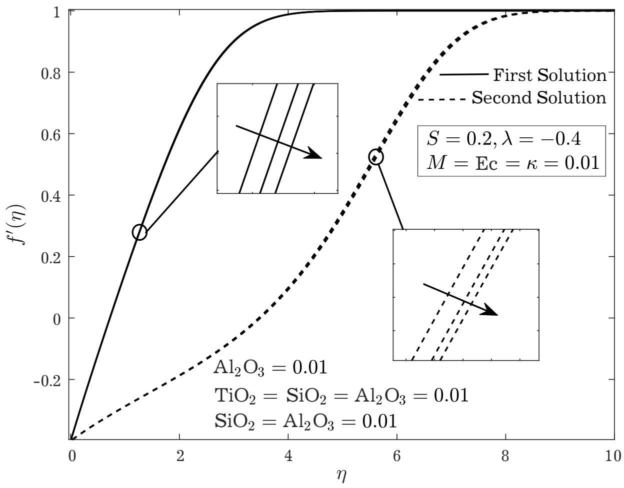

Fig. 6. Velocity profile with various ϕ.

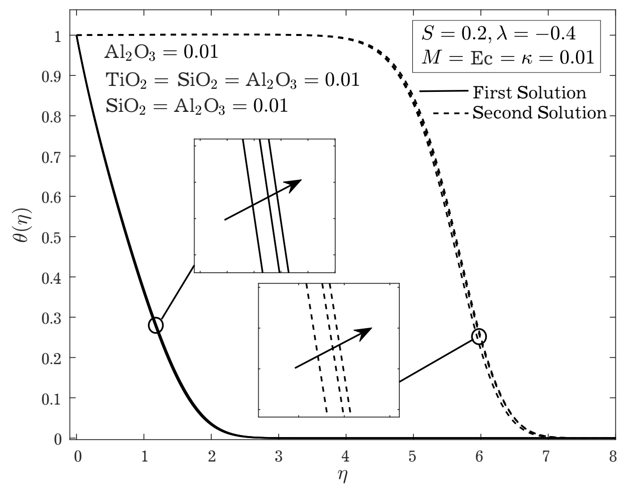

Fig. 7. Temperature profile with various ϕ.

Figures 6 and 7 then show the velocity $f'(\eta)$ and temperature $\theta(\eta)$ profile with various nanoparticles volume fraction when $S = 0.2$, $\lambda = -0.4$, $M = 0.01$, $\mathrm{Ec} = 0.01$ and $\kappa = 0.01$. Interestingly, SiO_2-Al_2O_3/H_2O has a slightly thicker momentum and thermal boundary layer thickness than Al_2O_3/H_2O. A higher-viscosity nanofluid experiences reduced momentum diffusion, resulting in a thicker momentum boundary layer. While, the temperature gradient within the boundary layer is influenced by the thermal conductivity of the nanofluid, leading to a broader thermal boundary layer. This result is consistent with those in Figures 4 and 5 when $\lambda = -0.4$ (opposing flow region).

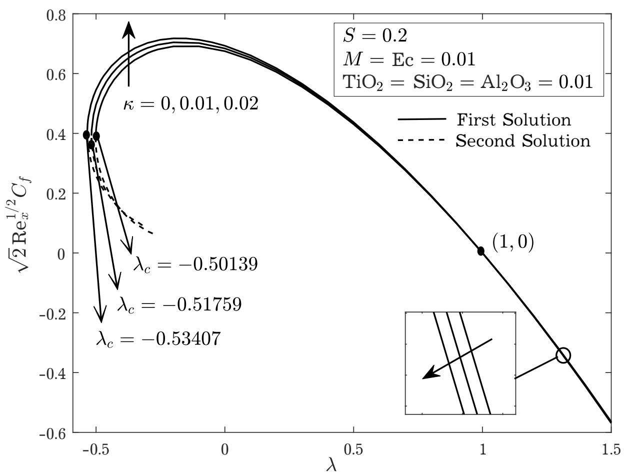

Fig. 8. Skin friction coefficient with various κ.

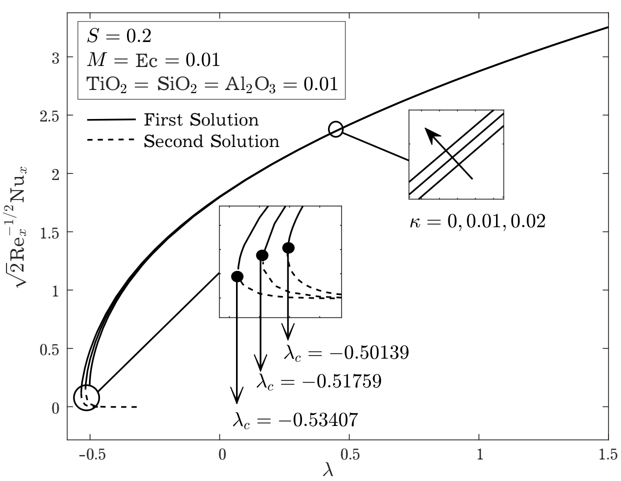

Fig. 9. Local Nusselt number with various κ.

Figures 8 and 9 show the variations of skin friction coefficient $\sqrt{2}\,\mathrm{Re}_x^{1/2}C_f$ and local Nusselt number $\sqrt{2}\,\mathrm{Re}_x^{-1/2}\mathrm{Nu}_x$ with different permeability of porous medium, which is $\kappa = 0,\ 0.01,\ 0.02$ when $S = 0.2$ for ternary nanofluid. Figures 10 and 11 then show the velocity $f'(\eta)$ and temperature $\theta(\eta)$ profile with various κ when $S = 0.2$, $\lambda = -0.4$, $M = 0.01$, $\mathrm{Ec} = 0.01$ and $\phi_1 = \phi_2 = \phi_3 = 0.01$. The obtained critical values of λ are $\lambda_c = -0.50139$, -0.51759 and -0.53407 when $\kappa = 0,\ 0.01,\ 0.02$. Hence, larger κ delays the boundary layer separation to happen. Physically, this happens because with increasing

κ, the porous medium becomes less permeable and due to this, the resistance force to the transport phenomenon becomes larger, which dominates the generated vorticity and maintains boundary layer for larger value of $|\lambda_c|$. Furthermore, the figure illustrates that the skin-friction coefficient, representing the surface drag force, escalates as κ increases for the upper branch solution when $\lambda_c < \lambda < 1$, whereas opposite outcome is found when $1 < \lambda \leqslant 1.5$. Increasing permeability allows fluid to flow more easily through the porous medium. With higher permeability, fluid flows faster through the porous medium. This increased flow velocity can result in higher shear stresses along the solid surface, leading to an increase in skin friction. In addition, it is seen from the figure that for the upper branch solution, heat transfer rate (local Nusselt number) increases with κ. As permeability increases, the fluid flows more rapidly through the porous medium. This enhanced fluid motion contributes to more efficient heat transfer through convective processes. It can be seen from Figures 10 and 11 that for upper solution branches, the momentum boundary layer becomes thinner with κ, while an opposite behavior is observed for lower branch solution. It is witnessed from the figure that for upper solution branches, the thermal boundary layer thickness shows decrement as κ grows. Also, it is fascinating to note that momentum and thermal boundary layer thickness for the lower branch solution is larger than that for the upper branch.

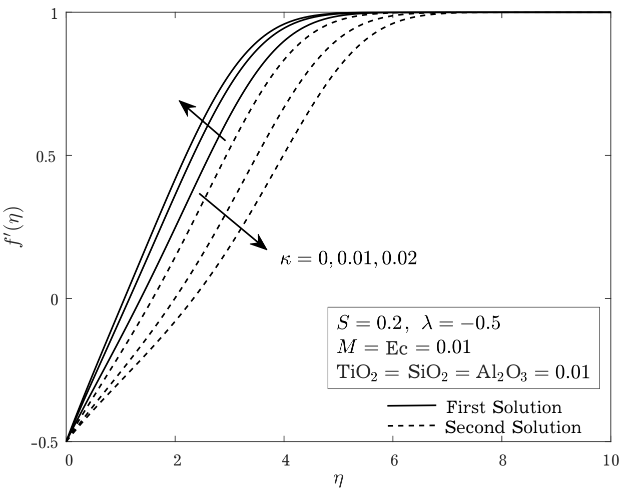

Fig. 10. Velocity profile with various κ.

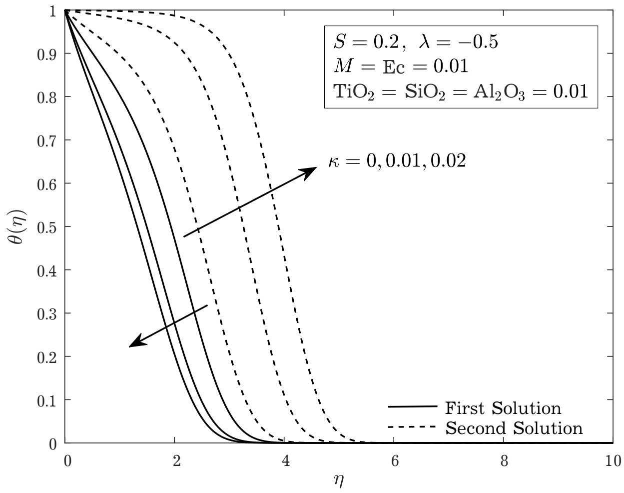

Fig. 11. Temperature profile with various κ.

5. Conclusion

The steady magneto-ternary nanofluid, TiO_2-SiO_2-Al_2O_3/H_2O flow in a porous medium over a moving plate with Joule heating is analyzed. The main findings of the current study are as follows:

— Dual solutions exist when the plate moves along a direction opposite to free-stream.
— Boundary layer separation from the plate is delayed with higher values of the permeability parameter κ and suction $S(> 0)$.
— The presence of nanoparticle volume fraction parameter shortens the range of solutions and fastens the boundary layer separation.
— Local skin-friction coefficient and local Nusselt number increases with increasing values of parameters S, κ and nanoparticle volume fraction.

[1] Choi S. U. S., Eastman J. A. Enhancing thermal conductivity of fluids with nanoparticles. Argonne National Lab. (ANL), Argonne, IL (United States) (1995).

[2] Suresh S., Venkitaraj K. P., Selvakumar P., Chandrasekar M. Synthesis of Al_2O_3–Cu/water hybrid nanofluids using two step method and its thermo physical properties. Colloids and Surfaces A: Physicochemical and Engineering Aspects. **388** (1–3), 41–48 (2011).

[3] Devi S. P. A., Devi S. S. U. Numerical investigation of hydromagnetic hybrid Cu–Al_2O_3/water nanofluid flow over a permeable stretching sheet with suction. International Journal of Nonlinear Sciences and Numerical Simulation. **17** (5), 249–257 (2016).

[4] Huminic G., Huminic A. Hybrid nanofluids for heat transfer applications – A state-of-the-art review. International Journal of Heat and Mass Transfer. **125**, 82–103 (2018).

[5] Manjunatha S., Puneeth V., Gireesha B. J., Chamkha A. Theoretical study of convective heat transfer in ternary nanofluid flowing past a stretching sheet. Journal of Applied and Computational Mechanics. **8** (4), 1279–1286 (2022).

[6] Shah N. A., Wakif A., El-Zahar E. R., Thumma T., Yook S.-J. Heat transfers thermodynamic activity of a second-grade ternary nanofluid flow over a vertical plate with Atangana–Baleanu time-fractional integral. Alexandria Engineering Journal. **61** (12), 10045–10053 (2022).

[7] Yahaya R. I., Ali F. M., Arifin N. M., Khashi'ie N. S., Isa S. S. P. M. MHD flow of hybrid nanofluid past a stretching sheet: double stratification and multiple slips effects. Mathematical Modeling and Computing. **9** (4), 871–881 (2022).

[8] Vishalakshi A. B., Kopp M. I., Mahabaleshwar U. S., Sarris I. E. Ternary hybrid nanofluid flow caused by thermal radiation and mass transpiration in a porous stretching/shrinking sheet. Mathematical Modeling and Computing. **10** (2), 400–409 (2023).

[9] Eid M. R., Mahny K. L. Flow and heat transfer in a porous medium saturated with a Sisko nanofluid over a nonlinearly stretching sheet with heat generation/absorption. Thermal Science and Engineering Progress. **47** (1), 54–71 (2018).

[10] Kameswaran P. K., Makukula Z. G., Sibanda P., Motsa S. S., Murthy P. V. S. N. A new algorithm for internal heat generation in nanofluid flow due to a stretching sheet in a porous medium. International Journal of Numerical Methods for Heat & Fluid Flow. **24** (5), 1020–1043 (2014).

[11] Eid M. R., Mahny K. L. Flow of viscoelastic ternary nanofluid over a shrinking porous medium with heat Source/Sink and radiation. Thermal Science and Engineering Progress. **40**, 101791 (2023).

[12] Kausar M. S., Hussanan A., Waqas M., Mamat M. Boundary layer flow of micropolar nanofluid towards a permeable stretching sheet in the presence of porous medium with thermal radiation and viscous dissipation. Chinese Journal of Physics. **78**, 435–452 (2022).

[13] Zeeshan A., Shehzad N., Atif M., Ellahi R., Sait S. M. Electromagnetic flow of SWCNT/MWCNT suspensions in two immiscible water-and engine-oil-based newtonian fluids through porous media. Symmetry. **14** (2), 406 (2022).

[14] Abu-Sitta A. M. M. A note on a certain boundary-layer equation. Applied Mathematics and Computation. **64** (1), 73–77 (1994).

[15] Wang L. A new algorithm for solving classical Blasius equation. Applied Mathematics and Computation. **157** (1), 1–9 (2004).

[16] Cortell R. Numerical solutions of the classical Blasius flat-plate problem. Applied Mathematics and Computation. **170** (1), 706–710 (2005).

[17] Idris S., Jamaludin A., Nazar R., Pop I. Heat transfer characteristics of magnetized hybrid ferrofluid flow over a permeable moving surface with viscous dissipation effect. Heliyon. **9** (5), e15907 (2023).

[18] Samat N. A. A., Bachok N., Arifin N. M. Carbon Nanotubes (CNTs) Nanofluids Flow and Heat Transfer under MHD Effect over a Moving Surface. Journal of Advanced Research in Fluid Mechanics and Thermal Sciences. **103** (1), 165–178 (2023).

[19] Aminuddin N. A., Nasir N. A. A. M., Jamshed W., Ishak A., Pop I., Eid M. R. Impact of Thermal Radiation on MHD GO-Fe_2O_4/EG Flow and Heat Transfer over a Moving Surface. Symmetry. **15** (3), 584 (2023).

[20] Khashi'ie N. S., Arifin N. M., Pop I. Magnetohydrodynamics (MHD) boundary layer flow of hybrid nanofluid over a moving plate with Joule heating. Alexandria Engineering Journal. **61** (3), 1938–1945 (2022).

[21] Makinde O. D., Aziz A. MHD mixed convection from a vertical plate embedded in a porous medium with a convective boundary condition. International Journal of Thermal Sciences. **49** (9), 1813–1820 (2010).

[22] Alharbi K. A. M., Ahmed A. E. S., Sidi M. O., Ahammad N. A., Mohamed A., El-Shorbagy M. A., Bilal M., Marzouki R. Computational valuation of Darcy ternary-hybrid nanofluid flow across an extending cylinder with induction effects. Micromachines. **13** (4), 588 (2022).

[23] Rohni A. M., Ahmad S., Pop I. Boundary layer flow over a moving surface in a nanofluid beneath a uniform free stream. International Journal of Numerical Methods for Heat & Fluid Flow. **21** (7), 828–846 (2011).

Аналіз теплообміну при потоці магнітної потрійної нанорідини в пористому середовищі по рухомій поверхні

Ануар Н. С.[1], Хуссейн Б. Н.[1], Асукі Н.А.М.[1], Бачок Н.[2,3]

[1]*Школа математичних наук, Коледж обчислювальної техніки, інформатики та математики, Університет технологій MARA, 40450 Шах Алам, Селангор, Малайзія*
[2]*Інститут математичних досліджень, Університет Путра Малайзія, 43400 Серданг, Селангор, Малайзія*
[3]*Кафедра математики та статистики, факультет природничих наук, Університет Путра Малайзія, 43400 Серданг, Селангор, Малайзія*

Дослідників привабили потрійні гібридні наночастинки через їх ефективність у посиленні теплообміну, і вони продовжують аналіз робочої рідини. Це дослідження присвячене потоку на магнітної потрійної нанорідини у пористому середовищі по рухомій пластині з джоулевим нагріванням. Для аналізу використовується комбінація TiO_2, SiO_2 і Al_2O_3 з водою, H_2O, як базовою рідиною. Використовуючи перетворення подібності, складність диференціальних рівнянь у частинних похідних (PDE) зводиться до систем звичайних диференціальних рівнянь (ODE), які потім чисельно розв'язуються в MATLAB за допомогою функції bvp4c для різних значень визначальних параметрів. Впливи різних безрозмірних фізичних параметрів на швидкість, температуру, а також на коефіцієнт поверхневого тертя та локальне число Нуссельта представлено у вигляді графіків. Два розв'язки досягаються, коли пластина та вільний потік рухаються вздовж протилежних напрямків. Крім того, локальне число Нуссельта збільшується з параметром проникності та параметром всмоктування. Крім того, збільшення параметра проникності та параметра всмоктування призводить до затримки відриву прикордонного шару. Крім того, завдяки поєднанню TiO_2 з об'ємним відсотком SiO_2–Al_2O_3/H_2O покращується передача тепла. Зі збільшенням об'ємної частки наночастинок подібність існуючих розв'язків зменшується.

Ключові слова: *потрійна нанорідина; течія граничного шару; теплообмін; пористе середовище; рухома пластина.*